




CHEMOSTRATIGRAPHY OF THE LOWER CRETACEOUS DINOSAUR-BEARING XIAGOU AND ZHONGGOU FORMATIONS, YUJINGZI BASIN, NORTHWEST CHINA

MARINA B. SUAREZ,^{*1} TIMOTHY MILDER,¹ NAN PENG,² CELINA A. SUAREZ,³ HAILU YOU,^{4,5} , DAQING LI,⁶ and PETER DODSON⁷

¹Department of Geological Sciences, The University of Texas at San Antonio, One UTSA Boulevard, San Antonio, Texas 78249, U.S.A., mb.suarez@ku.edu;

²Institute of Geology, Chinese Academy of Geological Sciences, 26 Baiwanzhuang Road, Beijing 100037, People's Republic of China;

³Department of Geosciences, University of Arkansas, 216 Gearhart Hall, Fayetteville, Arkansas 72701, U.S.A.;

⁴Key Laboratory of Vertebrate Evolution and Human Origins of Chinese Academy of Sciences, Institute of Vertebrate Paleontology and Paleoanthropology, Chinese Academy of Sciences, 142 Xizhimenwai Street, Beijing 100044, People's Republic of China;

⁵College of Earth Sciences, University of Chinese Academy of Sciences, Beijing 100049, People's Republic of China;

⁶Institute of Vertebrate Paleontology, Gansu Agricultural University, 1 Yingmencun, Anning District, Lanzhou City, Gansu Province 730070, People's Republic of China;

⁷Department of Biomedical Sciences, School of Veterinary Medicine, The University of Pennsylvania, 3800 Spruce Street, Philadelphia, Pennsylvania 19104, U.S.A.

ABSTRACT—The Early Cretaceous of northwest China has yielded abundant vertebrates, invertebrates, and plant fossils from numerous intermontane basins. Developing a chronostratigraphic context for these important fossil finds is important to understanding the development of modern terrestrial ecosystems, the evolution of dinosaurs, and the Cretaceous greenhouse climate. This study utilizes carbon isotope chemostratigraphy of the fossil-rich Xinminpu Group in the Yujingzi Basin in northwest Gansu Province. Lithostratigraphic descriptions defined three facies. The lowest is a tan, coarse arkosic sandstone, overlain by gray to variegated mudstones, sandstones, and thin limestones, which transition to red sandstones, conglomerates, and mudstones. Depositional environment interpretation of these lithofacies assisted in refining 450 samples of bulk sedimentary organic carbon as well as charcoal samples to develop a composite curve to correlate to existing carbon isotope curves from the region and to better constrained Cretaceous sections globally. The carbon isotope curve is correlated based on the broad positive excursion associated with carbon isotope fluctuations of the Paquier Episode that spans the late Aptian to early Albian. Based on this correlation, the middle gray mudstone facies, which contains a diverse fauna including theropods, sauro-pods, and ornithopods, as well as turtles and invertebrates, is placed within the upper Aptian. The upper red sandstone facies, which contains therizinosaurs and the ceratopsian dinosaur *Auroraceratops*, is placed in the lower Albian.

SUPPLEMENTAL DATA—Supplemental materials are available for this article for free at www.tandfonline.com/UJVP

Citation for this article: Suarez, M. B., T. Milder, P. Nan, C. A. Suarez, H. You, D. Li, and P. Dodson 2019. Chemostratigraphy of the Lower Cretaceous dinosaur-bearing Xiagou and Zhonggou formations, Yujingzi Basin, northwest China; pp. 12–21 in Hailu You, Peter Dodson, and Eric Morschhauser (eds.), *Auroraceratops rugosus* (Ornithischia, Ceratopsia) from the Early Cretaceous of northwestern Gansu Province, China. Society of Vertebrate Paleontology Memoir 18. Journal of Vertebrate Paleontology 38(Supplement). DOI: 10.1080/02724634.2017.1510412.

INTRODUCTION AND BACKGROUND

Northwest China has been a focus of fossil discovery from continental paleoenvironments of the Cretaceous since at least the late 1900s (Bohlin, 1953; Hou and Liu, 1984; Jerzykiewicz and Russell, 1991; Tang et al., 2001; You et al., 2005, 2006, 2010; Ji et al., 2011). Exquisitely preserved fossils include early birds, nonavian dinosaurs, mammals, turtles, fish, plants, insects, and other invertebrates (Tang et al., 2001; You et al., 2006). The Cretaceous was a time of modernization (diversification of flowering plants, birds, mammals, and many insects) of terrestrial ecosystems (Lloyd et al., 2008) and was also a time of overall global

warmth (Hay and Floegel, 2012). Asia, being the largest continent during the Cretaceous, is important for understanding changes in terrestrial ecosystems and climate. It is host to the greatest diversity of Mesozoic birds as well as many early angiosperms (Sun et al., 2011; Wang et al., 2015) and provides a large spatial and temporal record for the understanding of Cretaceous climate (Sewall et al., 2007; Hasegawa et al., 2012). To elucidate the timing of potential triggers and responses of continental environmental changes, improved stratigraphic constraints are necessary. Here, we present a stable carbon isotope chemostratigraphic profile obtained from samples collected from the fossiliferous Yujingzi Basin in northwest Gansu Province.

Use of carbon isotope curves to correlate terrestrial strata to time-equivalent marine strata has been successful in a number of localities (Gröcke et al., 1999; Heimhofer et al., 2003; Ludvigson et al., 2010, 2015) due to the fact that the

*Corresponding author.

Color versions of one or more of the figures in the article can be found online at www.tandfonline.com/ujvp.

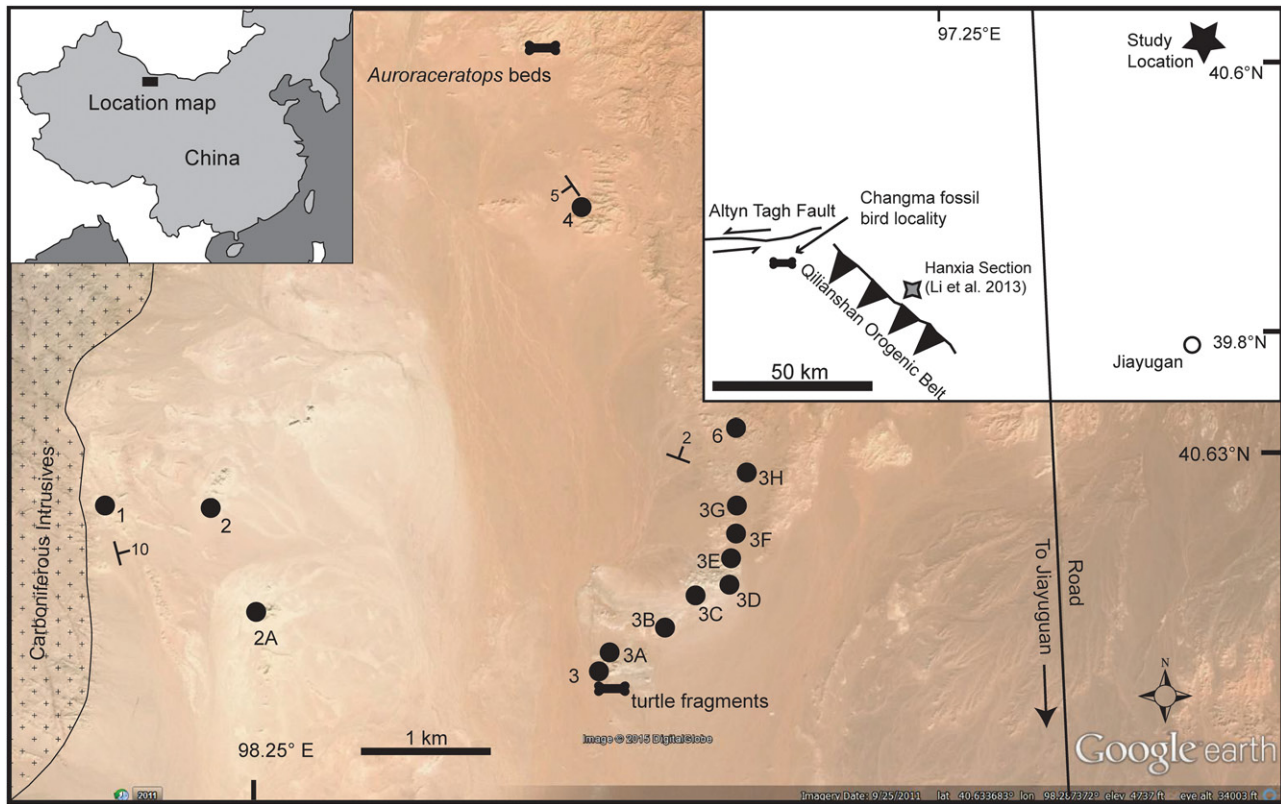


FIGURE 1. Aerial photography (Google Earth, 2015) and locations of measured sections. Left inset map of China shows the Yujingzi Basin location. Right inset map shows the study area (star) in relation to another fossil locality (the Changma fossil bird locality), and the Hanxia section locality of Li et al. (2013), from which radiometric dates were obtained.

Cretaceous Period experienced a number carbon cycle perturbations that are reflected in the partitioning of ^{12}C and ^{13}C in different carbon reservoirs (Jenkyns, 2010). In marine sequences, these perturbations are often associated with organic-rich shales that are interpreted as oceanic anoxic events (OAEs) (Schlanger and Jenkyns, 1976; Scholle and Arthur, 1980). Oceanic anoxic events are often (although not exclusively) preceded by negative carbon isotope excursions and are concurrent with positive isotope excursions (Jenkyns, 2003, 2010). Negative excursions have been variously interpreted as (1) the result of a release of methane clathrates similar to that responsible for the Paleocene–Eocene Thermal Maximum (Jahren, 2001; Jenkyns, 2003); (2) increased upwelling and recycling of ^{12}C -rich intermediate marine waters or ^{12}C -enriched HCO_3^- from bacterial sulfate reduction; (3) enhanced continental runoff; (4) volcanic CO_2 ; (5) poor ecological conditions for pelagic calcareous organisms resulting in a disruption in the partitioning of carbon isotopes between carbonate and organic carbon reservoirs; (6) enhanced oxidation of terrestrial organic matter; or (7) a decrease in primary productivity (biological carbon pump) (Menegatti et al., 1998; Föllmi, 2012). Positive carbon isotope excursions are thought to represent increased organic carbon burial and sequestration of the ^{12}C in organic material (Scholle and Arthur, 1980; Jenkyns, 2010). This leaves the remaining pool of carbon in surface ocean water enriched in the heavier isotopes of carbon (^{13}C). The pattern of the positive and negative isotope excursions can be correlated to continental sequences because isotopic exchange between the larger surface ocean carbon reservoir and the atmospheric carbon reservoir (atmospheric CO_2) occurs quickly (74 gigatons/

year), as does the exchange between atmosphere and terrestrial vegetation (100 gigatons/year) (Ruddiman, 2008). Because exchanges occur relatively quickly in the active carbon cycle, carbon isotope events recorded in continental and marine environments occur synchronously at geologic time scales. The isotopic composition of sedimentary organic matter in continental depositional systems is dominated by plant material, whose isotopic composition originates from the carbon isotopic composition of CO_2 plus a fairly consistent offset for C3 photosynthesis (approximately -18‰ to -19.5‰ relative to atmospheric $\delta^{13}\text{C}$ values) (Koch, 1998; Ekart et al., 1999). Although a number of effects can vary this photosynthetic offset, the general trends between marine carbon isotope and continental isotope records should vary concurrently. This study focuses on developing a carbon isotope curve from the C3-dominated ecosystem of fossiliferous continental deposits from the Yujingzi Basin in order to correlate the deposits to other Early Cretaceous strata and more accurately constrain the age of the units.

GEOLOGIC SETTING

The Yujingzi Basin is located in northwestern China, in the province of Gansu, approximately 100 km north-northwest of the city of Jiayuguan (Fig. 1). The intermontane basins of the Hexi Corridor in Gansu Province are the result of strike-slip basins that accommodate motion occurring during the collision of the Lhasa Block with Asia (Chen and Yang, 1996; Vincent and Allen, 1999). Within the study area, the Cretaceous

Xinminpu Group forms a nonconformity with underlying Carboniferous granites (pers. observ.; Nan et al., 2011).

In northwest China, Lower Cretaceous strata are assigned to the Xinminpu Group, which consists of four formations in the following stratigraphic order: the Chinjinqao Formation, the Chinjinpu Formation, the Xiagou Formation, and the Zhonggou Formation (Vincent and Allen, 1999; Tang et al., 2001; You et al., 2005; Morschhauser, 2012; Kuang et al., 2013). Localities to the south of the Yujingzi Basin with strata identified as the Xinminpu Group have been sampled for radiometric dates and have yielded ages ranging from 123 ± 2.6 to 113.7 ± 1.8 Ma (Kuang et al., 2013; Li et al., 2013).

Within the study area, only the Xiagou and Zhonggou formations are exposed (Nan et al., 2011). The Xiagou Formation consists of gray to gray-green mudstones and siltstones interbedded with sandstones and conglomerates (Chen and Yang, 1996; You et al., 2005; pers. observ., 2011). The Zhonggou Formation consists of relatively coarser clastics, such as purple to red conglomerates and coarse sandstones interbedded with gray-green siltstones and mudstones and yellow sandstones (Chen and Yang, 1996; You et al., 2005; pers. observ., 2011; Li et al., 2013).

MATERIALS AND METHODS

Stable carbon isotope ratios for bulk sedimentary organic carbon were determined for 550 samples selected for this study from 13 sections (Fig. 1). Samples were collected at 25–100-cm intervals over approximately 320 m of section; fine-grained lithologies were sampled at intervals of 25 cm, and coarse-grained sediments were sampled at greater intervals, of 50–100 cm, to accommodate this coarse sediment, which is assumed to have had a higher sedimentation rate than the floodplain and lacustrine environments (Schindel, 1980; Enos, 1991). Samples were individually powdered and homogenized by hand and acidified in 3 M HCl at 60°C for 2 hours to remove carbonate and sulfurous material (Midwood and Boutton, 1998; Robinson and Hesselbo, 2004). Samples were subsequently rinsed and dried. Between 5 and 135 mg of the dried sample material was weighed into tin capsules. Carbon isotopic compositions were determined by combustion via a Costech ECS 4010 elemental analyzer coupled to a ThermoFinnigan Delta Plus XP isotope ratio mass spectrometer in the Department of Geological Sciences at the University of Texas at San Antonio. Sample isotopic values are corrected for size, drift, and source stretching effects and reported relative to the Vienna Pee Dee Belemnite (VPDB) international standard by using international standards sucrose (International Atomic Energy Agency (IAEA) C-6, formerly ANU (Australian National University) sucrose, caffeine (IAEA 600), and United States Geological Survey (USGS) 24 graphite. External precision is determined to be $\pm 0.1\%$ by routine measurement of National Institute of Standards and Technology (NIST) 1547 (Peach Leaves). Replicate and triplicate analyses of samples resulted in an average standard deviation of 0.6‰.

Samples with very low percentages of organic carbon (Sections 2, 2A, and 4) values were analyzed at the Keck Paleoenvironmental and Environmental Stable Isotope Laboratory at the University of Kansas. These samples were combusted on a Costech ECS 4010 elemental analyzer coupled to a ThermoFinnigan MAT 253 isotope ratio mass spectrometer. Montana Soil (NIST Reference Material 2711) and Peach Leaves (NIST Reference Material 1547) standards were used to determine precision. Results compiled over 2 years show the precision to be better than $\pm 0.22\%$.

FACIES DESCRIPTION AND INTERPRETATION

Facies Descriptions

We recognize three general facies associations, schematically shown in Figures 2 and 3. The stratigraphically lowest facies association is represented by Sections 1, 2, and 2A. Overlying this, Sections 3, 3A–H, and 6 are grouped as a second facies association and a third facies is represented by Section 4.

The facies association represented by Sections 1, 2, and 2A consists of tan, red, and gray-green, coarse-grained, angular arkosic sandstones and conglomerates derived from the underlying Paleozoic granites. From a distance, these facies appear as white hills and pinnacles (Fig. 3A). These sandstones tend to be sheet-like in geometry and are poorly-sorted, with grain sizes ranging from fine sands and silts with some clays to pebble conglomerates. Within Section 2, there are occasional meter-scale or thinner clay-rich beds that are characterized by color mottling and slickensides.

Modern colluvium covers the transition from the stratigraphically lowest facies to the overlying facies association represented by Sections 3, 3A–H, and 6. These facies consist of alternating beds of gray and variegated mudstones and muddy sandstones every few meters (Fig. 3B, C, E). The lowermost part of this facies (Section 3) consists of dark greenish-black mudstones with organic fragments and turtle remains. Thin, massive to nodular limestones are interbedded with mudstones. Charophytes, ostracodes, and gastropods occur in the mudstones and muddy sandstones. Within this facies association, a number of red and gray-green mudstones are characterized by the presence of carbonate nodules, root traces, horizonation, and curvilinear slickensides (Fig. 3B). The red and gray-green mudstones occur between meter-scale, typically coarse quartz sandstones that are generally poorly lithified. Some sandstones fine upward, whereas others are generally massive. Many of the sandstones contain rip-up clasts from underlying mudstones and are poorly sorted.

Section 4 consists of coarse-grained, poorly sorted arkosic sandstones and sandy mudstones. This section is noticeably redder with slickensides, color mottling, root traces, carbonate nodules, burrows, and blocky ped structures (Fig. 3D–F). It is from these facies that the majority of the *Auroraceratops* skeletons have been recovered (Morschhauser, 2012).

Facies Interpretations

Based on the generally immature nature of the facies associated with Sections 1, 2, and 2A, we interpret these sections to have been deposited in a dominantly alluvial fan environment with minor paleosol development. The overlying facies (Sections 3, 3A–H, and 6) is interpreted to represent fluvio-lacustrine and palustrine environments. Lacustrine to palustrine environments are recognized by the presence of turtle remains, charophyte, gastropod, and ostracode remains, gleyed to dark, organic-rich mudstones, and thin limestones. Sandstones represent fluvial deposits and are interbedded and modified by soil development. Fluvial sands are represented by lenticular sands, typically fining up with erosive bases that include rip-up clast from underlying strata. Soils are recognized by the presence of horizonation, slickensides, root traces, and carbonate nodules that are interpreted to be pedogenic in origin. The clay-rich slickensides in paleosols are typically the result of wetting and drying, indicating a seasonal climate. In addition, the crisscrossed, curvilinear nature of these slickensides results in structures interpreted as mukarra structures and gilgai microrelief (Fig. 3B), which are diagnostic of vertisols (Retallack, 1997). Carbonate nodules typically form in sub-humid to semiarid environments when mean annual

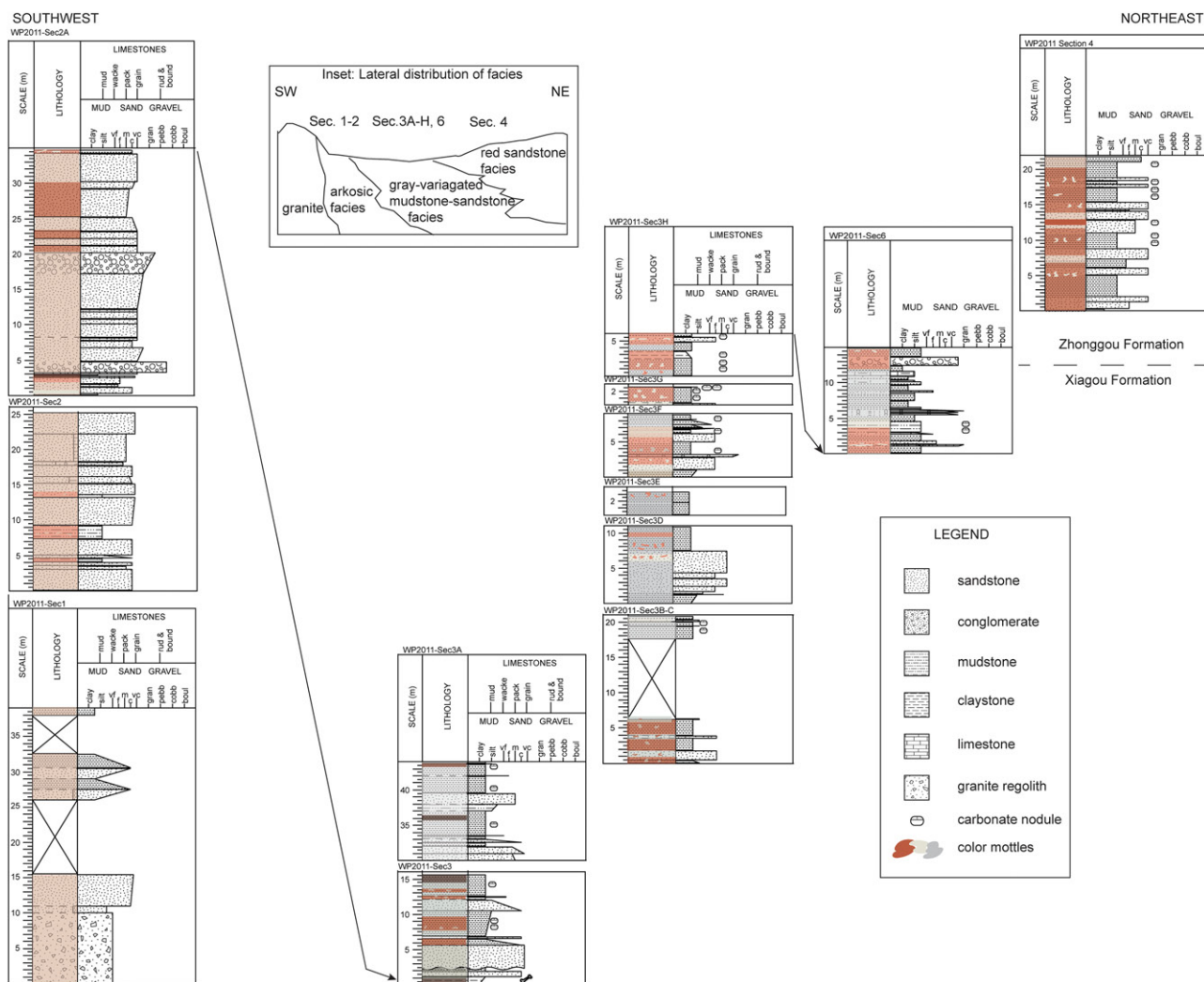


FIGURE 2. Lithology and lateral distribution of measured sections. Note: horizontal distances are not to scale. The boundary between the Xiangou and Zhonggou formations is proposed to occur at a meter-scale conglomerate in Section 6. Inset diagram shows the suggested lateral distribution and relationship between facies.

precipitation is less than 50–60 cm per year, although they can occur at higher precipitation rates in distinctly seasonal climates such as monsoonal climates (Birkeland, 1999; Srivastava, 2001; Breecker et al., 2009). The facies represented by Section 4 and those of Morschhauser (2012) are interpreted as fluvial-overbank environments based on the predominantly sandstone facies interbedded with paleosols and carbonate nodules. The strata are considerably redder and lack gleyed colors, suggesting that soils were better drained than paleosols in the second facies association.

ISOTOPE RESULTS AND INTERPRETATIONS

Isotope Results

The stable isotopic composition of bulk sedimentary organic carbon averages -24.2‰ in the Yujingzi Basin and ranges from a minimum of -29.8‰ to a maximum of -20.5‰ (Fig. 4). The lithofacies present in the Yujingzi Basin represents a wide range of continental depositional environments. As a result, investigation of carbon isotope values and their relationship to

these depositional environments is warranted. Figure 4 shows the distribution of $\delta^{13}\text{C}$ values stratigraphically and by depositional environment. The values tend to be lower in Sections 1, 2, and 2A (both paleosol deposits and the dominantly alluvial fan deposits). The middle section in all facies shows a decrease and increase over a short stratigraphic interval, followed by a longer-term decrease from near the top of Section 3 to Sections 3A and 3B. There are a number of breaks in the section where samples were not collected, so this trend is tentative. There is more variability in the paleosol values than in the charcoal, lacustrine/palustrine, and fluvial samples. From Sections 3C to 3H, there is a broad increase and decrease in $\delta^{13}\text{C}$ values in the paleosol and fluvial facies. The broad increase is interrupted by two short decreases, whereas there is only one prominent decrease in the charcoal values. The lacustrine/palustrine and fluvial trends are more muted, with lacustrine/palustrine facies showing an overall increase to the top of Section 6. Meanwhile, the paleosol and fluvial values show an increase and decrease in Section 6. Within Section 4, paleosol facies and fluvial facies show an overall increase.

Statistical comparisons of the carbon isotope values from each facies representing different depositional environments

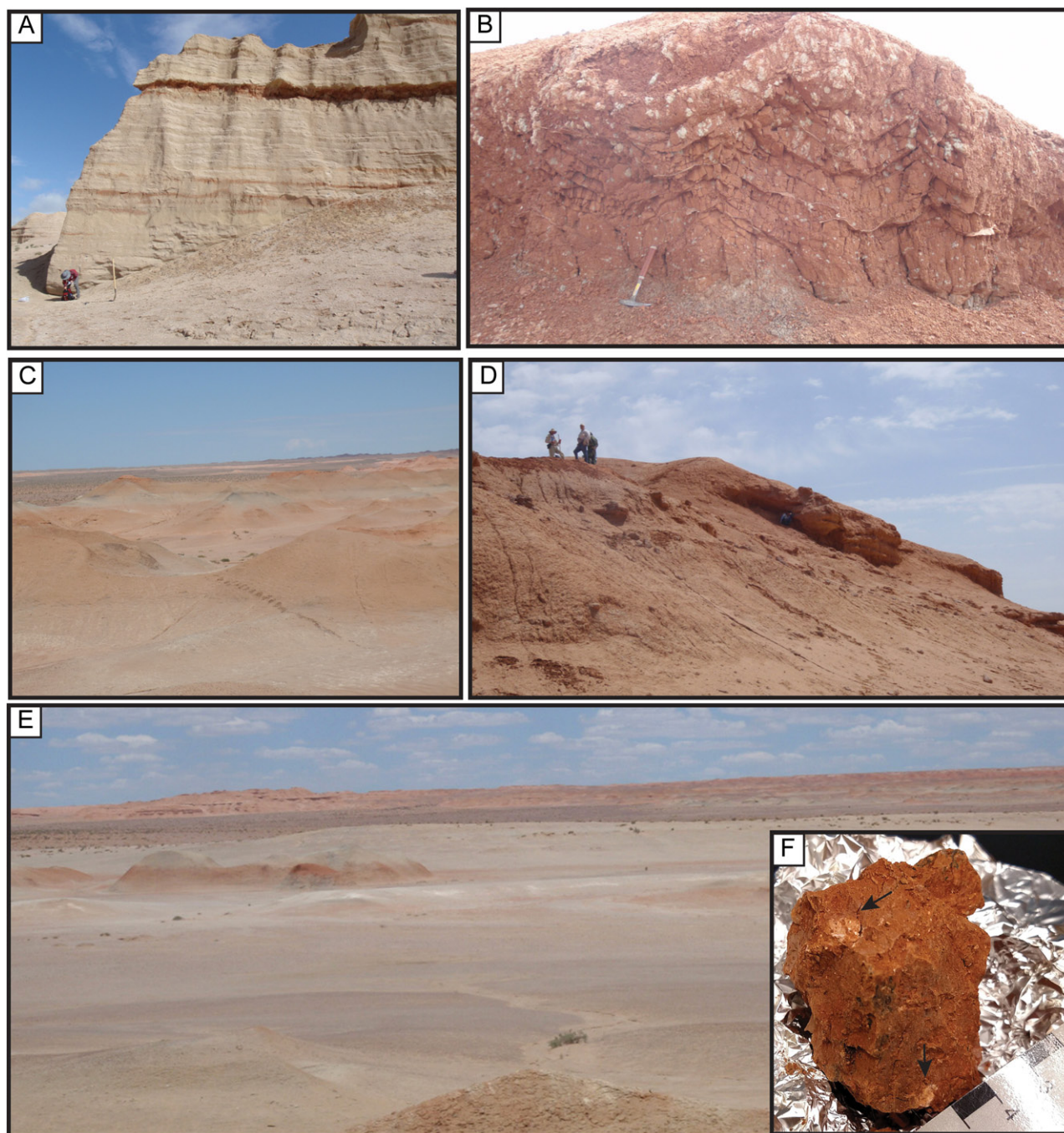


FIGURE 3. Outcrop photographs of the Xinminpu Group in the Yujingzi Basin. **A**, lower arkosic facies also known as ‘white pagodas.’ Arkosic sandstones are sheet-like in geometry. **B**, curvilinear slickensides in the gray to variegated middle facies. White nodules are carbonate nodules. **C**, overview of variegated beds in the middle facies. **D**, upper red sandy facies with resistant beds composed of lenticular sandstone beds. **E**, overview of middle gray to variegated facies with upper red sandy facies in the distance. **F**, ped structure with small carbonate nodules from the upper red sandy facies. Arrows point to carbonate nodules.

were conducted using Kruskal-Wallis analysis of variance (ANOVA). The depositional environments that were compared were alluvial, fluvial, overbank (paleosol), and lacustrine (palustrine was grouped with lacustrine). In addition, a number of charcoal samples were also analyzed and compared. At the 95% confidence level, all depositional environments were significantly different from each other. The paleosol and charcoal $\delta^{13}\text{C}$ values, however, were not significantly different from each other. This is important because it suggests that the $\delta^{13}\text{C}$

values of the paleosols are primarily controlled by the $\delta^{13}\text{C}$ of vegetation, which is determined by the $\delta^{13}\text{C}$ value of the atmosphere offset by C3 photosynthesis. The fact that the carbon isotope values from each of the different depositional environments are significantly different from each other indicates that all $\delta^{13}\text{C}$ values cannot be used in the comparison of these data with global data sets. Another aspect to test is the variability of the $\delta^{13}\text{C}$ values with respect to %C as well as grain size. Figure 5 shows the correlations between grain size and

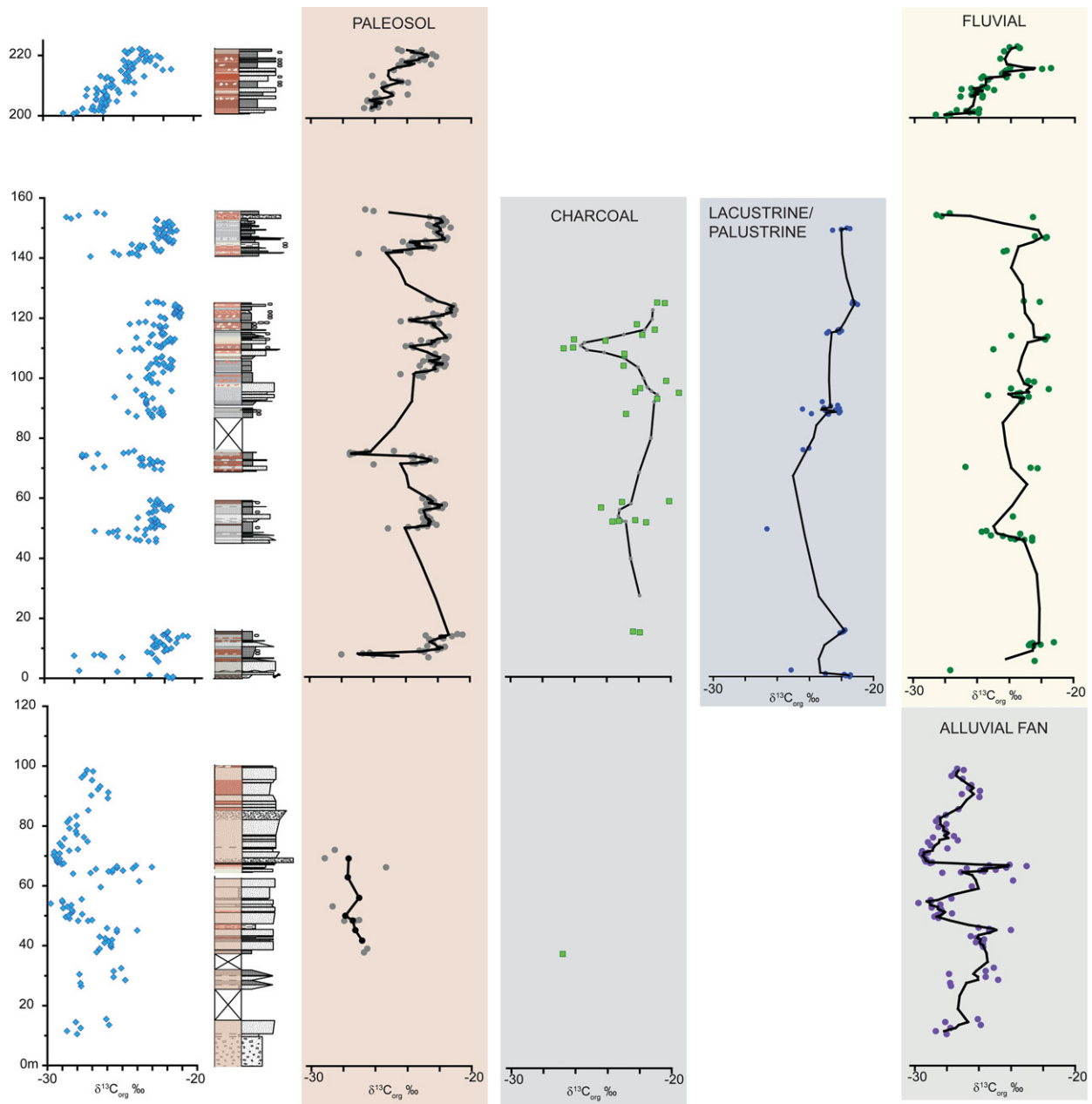


FIGURE 4. Carbon isotopic compositions of strata from the Yujingzi Basin. On the left are all $\delta^{13}\text{C}_{\text{org}}$ values for sedimentary organic carbon. The lithostratigraphic columns from Figure 2 are also provided. From left to right are the $\delta^{13}\text{C}_{\text{org}}$ values of samples separated by depositional environment interpretation. These include paleosols, charcoal, lacustrine, and palustrine environments, fluvial environments, and alluvial environments.

$\delta^{13}\text{C}$ values as well as %C. Grain size does not appear to show a strong correlation; however, sandstones (average = -25.7‰) and conglomerates (average = -26.2‰) are on average lower than limestones (-23.7‰) and claystones and mudstones (-23.2‰). An analysis using Kruskal-Wallis ANOVA suggests that the $\delta^{13}\text{C}$ values of limestones, mudstones and claystones, sandstones, and conglomerates are significantly different from each other. A potential reason for this is that the organic matter recovered from sandstones and conglomerates may represent plants that are less water stressed, a factor that tends to cause enrichment in $\delta^{13}\text{C}$ values of plants (Kohn, 2010). By filtering out fluvial-derived $\delta^{13}\text{C}$ values, this artifact may be eliminated from complicating the correlation (see below). The

majority of the samples are of low %C. There is no strong correlation between %C and $\delta^{13}\text{C}$ (correlation coefficient = 0.28). Only a few samples seem to be high in %C. These primarily come from lacustrine-palustrine samples and tend to be more enriched in ^{13}C . These samples were not included when making comparison between the Yujingzi Basin chemostratigraphic curve and other curves (see below).

Carbon Isotope Correlations

Correlations of chemostratigraphic profiles are greatly aided when used in conjunction with other chronostratigraphic methods. Attempts to find ashes or detrital zircons in the Yujingzi

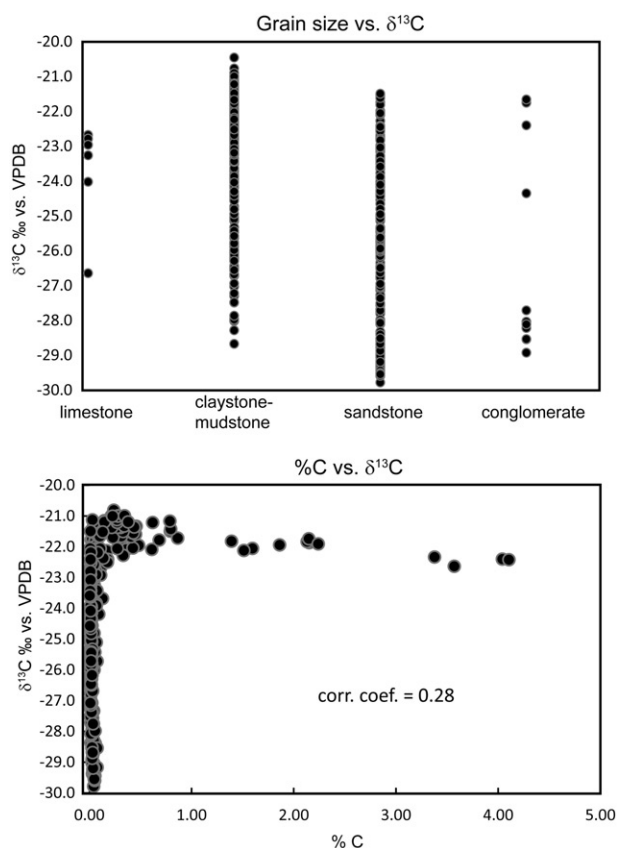


FIGURE 5. Grain size and %C relationships to $\delta^{13}\text{C}$. Grain size shows no significant relationship with the $\delta^{13}\text{C}$ of sedimentary organic carbon. %C shows a very weak correlation with $\delta^{13}\text{C}$ (correlation coefficient = 0.28). The few samples that have higher than 1% C are primarily from strata interpreted to be lacustrine. These samples were filtered out from the chemostratigraphic curve so as not to bias the correlation.

Basin have unfortunately been unsuccessful; however, work in adjacent basins in Gansu provides some insight. Tang et al. (2001) reports palynomorphs suggestive of Early Cretaceous, possibly Albian, in the nearby Gongpoquan and Suanjingzi basins. In a neighboring basin to the south of the Yujingzi Basin, the Hanxia basin, Li et al. (2013) report U-Pb ages from single zircon crystals derived from basalts. These yield an age of 115 ± 4.5 Ma approximately 60 m above the base of the Zhonggou Formation at that locality and an age of 123 ± 2.6 Ma approximately 240 m above the base of the Xiagou Formation. In another study, Kuang et al. (2011) report two radiometric ages from Hanxia and Hongliuxia basalts near the Xiagou-Zhonggou contact. These values are 113.7 ± 1.8 and 115.6 ± 1.1 Ma. The current (2012) Geologic Time Scale (Ogg and Hinnov, 2012) places the base of the Aptian stage at 126.3 Ma. The Aptian–Albian boundary has yet to be numerically defined but is currently placed at 113 Ma. Based on these numerical and biostratigraphic age constraints, comparison of the Yujingzi Basin carbon isotope chemostratigraphic curve should be restricted to carbon isotope excursions that occur in the Aptian to early Albian.

Significant variability occurs throughout the raw $\delta^{13}\text{C}_{\text{org}}$ curve (Fig. 4). This is expected for a dynamic landscape such as a floodplain environment (Hoffman et al., 2009; Samaritani et al., 2011; Baczynski et al., 2013). Because (1) they represent the majority of the $\delta^{13}\text{C}$ data points and (2) they are not significantly different from the charcoal samples,

chemostratigraphic correlations will be compared using only paleosol and charcoal $\delta^{13}\text{C}$ values. To correlate the chemostratigraphic records from the Yujingzi Basin, a composite section of bulk organic matter and charcoal was constructed along with a 3-point running average of the data. Figure 6 correlates trends of the composite Yujingzi Basin section to Aptian–Albian records of a composite $\delta^{13}\text{C}$ curve from terrestrial carbonates from Li et al. (2013) of northwest China basins, an organic $\delta^{13}\text{C}$ curve of Bralower et al. (1999) from shallow marine rocks from northeastern Mexico, and an organic $\delta^{13}\text{C}$ curve of Heimhofer et al. (2003) from coastal sediments of the Algarve Basin, Portugal. In the Yujingzi Basin, attention is especially paid to positive and negative trends that are greater than about 1.9‰ (the standard deviation of paleosol and charcoal $\delta^{13}\text{C}$ data).

Correlation is based on the broad positive excursion that occurs in the middle of the section. This resembles the shape of the broad positive curve of Li et al. (2013) that spans the Aptian–Albian boundary. In addition, it resembles the C9–C11 carbon isotope segments defined by Bralower et al. (1999) and the positive curve in terrestrial organic matter of Heimhofer et al. (2003). This correlation is shown in Figure 6 as the yellow-highlighted segment across these isotope curves. A comparison with the 2012 Geologic Time Scale (Ogg and Hinnov, 2012) suggests that this broad positive isotope excursion lasted no longer than about 4 million years.

The prominent positive isotope peak below this broad positive excursion is tentatively correlated to the lowermost positive excursion in the Li et al. (2013) composite section, which is correlated to the positive C7 isotope excursion of Bralower et al. (1999). This is the positive isotope excursion that is associated with the early Aptian Selli Event (Menegatti et al., 1998). This excursion is noted by the dashed red line in Figure 6. The next prominent positive peak above the broad C10 positive excursion that occurs near the top of the middle section (Section 6) is tentatively correlated (short dash blue line) to the next positive excursion of Li et al. (2013). This appears to represent the C12 positive excursion, which is somewhat more muted than the broad C10 positive excursion. These correlations are tentative (and hence dashed in Fig. 6) because gaps in data occur above or below these peaks in $\delta^{13}\text{C}$ values.

The transition from the Xiagou Formation to the Zhonggou Formation is believed to occur in the Yujingzi Basin, with the majority of the dinosaur localities occurring in the Zhonggou Formation. Morschhauser (2012) after Li (2008) does not distinguish between the Xiagou and Zhonggou formations but does identify two faunas, one in the ‘lower unit’ that consists of a diversity of dinosaurs, including basal hadrosauroids, titanosaurs, ornithomimid, and the basal neoceratopsian dinosaur *Archaeoceratops*. The ‘middle unit’ consists primarily of *Auroraceratops* and the therizinosaur *Suzhousaurus*. This ‘middle unit’ correlates to our Section 4. The contact between the Zhonggou Formation and underlying Xiagou Formation in the Hanxia section of Li et al. (2013) is marked by a conglomerate. A number of conglomeratic beds occur in Section 6, with the thickest being approximately 1 m in the upper part of the section, just above a negative trend in the carbon isotope curve. The carbon isotope chemostratigraphy at the Hanxia section (Li et al., 2013) is of low resolution, but the conglomerate associated with the base of the Zhonggou Formation also occurs during a negative phase in the $\delta^{13}\text{C}$ chemostratigraphic record. Based on the chemostratigraphic and lithostratigraphic record of this study, the study of Li et al. (2013), and the stratigraphic descriptions of Morschhauser (2012) after Li (2008), the more diverse fauna of the ‘lower unit’ is assigned to the Xiagou Formation and the fauna of the ‘middle unit’ is assigned to the Zhonggou Formation.

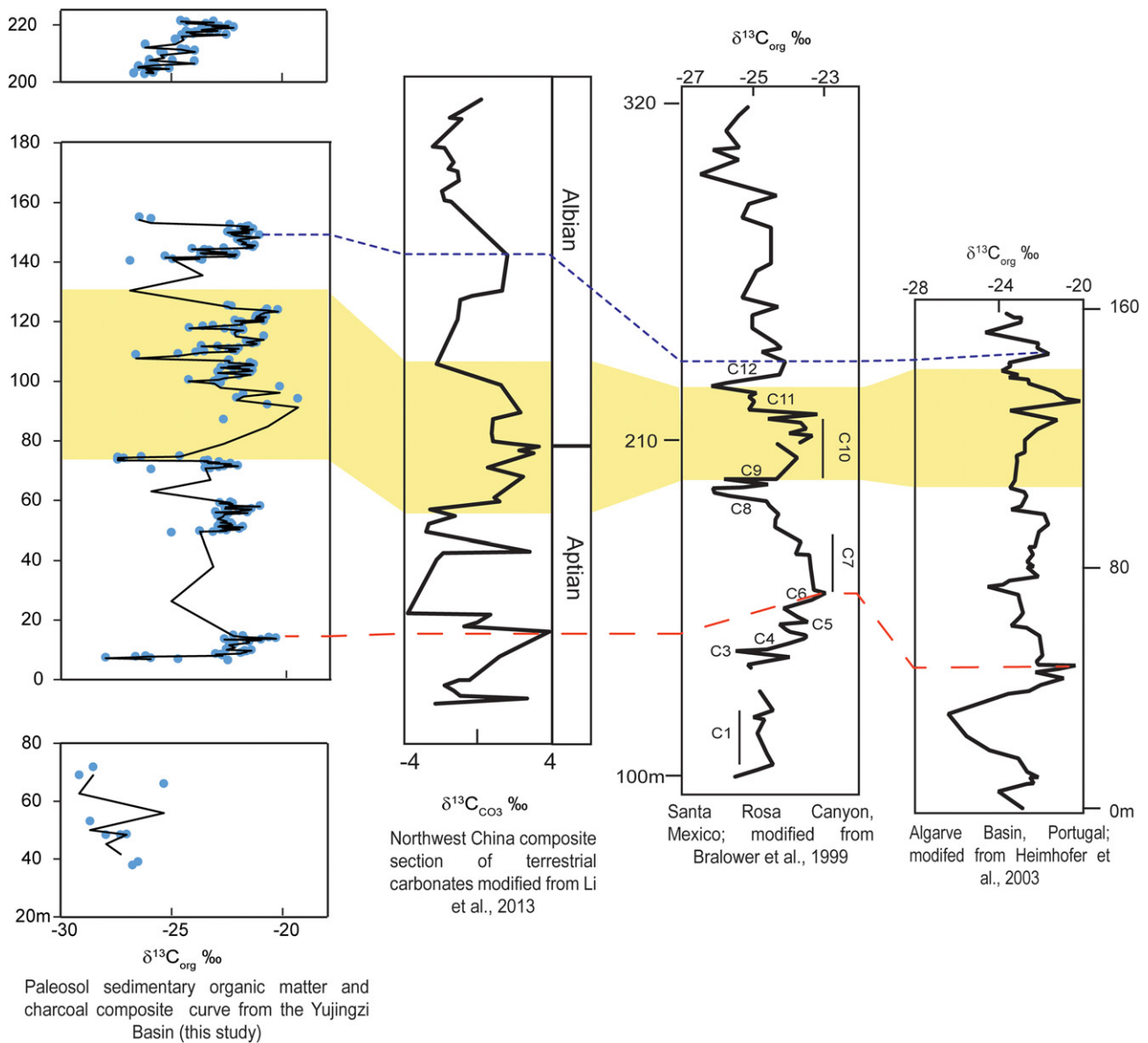


FIGURE 6. Composite chemostratigraphic curve from the Yujingzi Basin consisting of data and 3-point moving average (solid line) from paleosol and charcoal samples. Correlation to the composite curve of Li et al. (2013) is based on the broad positive isotope excursion that occurs in the middle portion of the variegated facies and is highlighted here in yellow. The curve of Li et al. (2013) is a composite from carbonates of multiple northwest China basins constrained by radiometric dates. The curve is also correlated to the sedimentary organic carbon curve of Bralower et al. (1999), which depicts carbon isotope segments C1–C12 (after Menegatti et al., 1998, and Bralower et al., 1999) from Mexico and the sedimentary organic carbon curve of Heimhofer et al. (2003) from Portugal. The red dashed line is tentatively correlated to the positive isotope excursion C7. This is tentative because there are significant gaps above and below the positive excursion denoted by the red dashed line in our composite data set. The blue short-dash line is tentatively correlated to a smaller positive isotope excursion after the C10 positive isotope excursion. This is tentative because of the gap in data, especially above the positive excursion in our composite data set denoted by the blue short-dash line.

An advantage of chemostratigraphic correlation is that not only can it constrain correlative rock units, but the underlying causes of carbon isotope excursions are related to carbon cycle fluctuations and interaction between the ocean and atmospheric systems. These changes can be used to determine the response (if any) of continental ecosystems to these carbon cycle perturbations (Ludvigson et al., 2010, 2015; McInerney and Wing, 2011; Föllmi, 2012). The C9–C12 carbon isotope segments of Bralower et al. (1999) encompass ocean anoxic event 1b (OAE 1b), also termed the Paquier Episode, which

occurred in the latest Aptian to early Albian. Recent reviews of the carbon isotope fluctuations associated with the late Aptian to early Albian have suggested warm humid conditions (Jenkyns, 2010; Föllmi, 2012), although there are other interpretations suggesting that cooler, arid conditions interrupted the overall warm and humid environments. Friedrich et al. (2005), for example, suggested overall humid conditions, but distinct cooling and drying conditions based on changes in populations of Tethyan benthic foraminifera. From a review of continental strata, Hasegawa et al. (2012) suggested that the

subtropical high-pressure zone shifted equatorward, bringing more humid conditions further south over much of Asia during the mid-Cretaceous (Aptian to Turonian). Recently, Ludvigson et al. (2015) investigated the C10 positive excursion from the Aptian to Albian continental strata of the coeval Cedar Mountain Formation of Utah, U.S.A., suggesting that the C10 excursion coincides with increased aridity, which may have been a result of increased temperatures due to CO₂ output from large igneous provinces. The facies of the Xiagou Formation (and those that fall within the C10 interval identified in the Yujingzi Basin) fluctuate between more water-saturated conditions (lacustrine to palustrine environments) and dryer and well-drained red paleosols. The more diverse fauna is consistent with a warm, humid environment as suggested by Hasegawa et al. (2012) but contrasts somewhat with the findings of Ludvigson et al. (2015), who suggested increased aridity during the C10 interval. The increase in the occurrence of red paleosols up section and the presence of pedogenic carbonate nodules do suggest increased aridity, and the less diverse fauna of the Zhonggou Formation may suggest a response to this environmental change. Other studies have suggested that carbon cycle-induced climate fluctuations have resulted in faunal changes on land (Retallack, 2009; Föllmi, 2012). More detailed assessment of faunal changes and more quantitative paleoclimate proxies from the Yujingzi Basin should (and will) be carried out to test such hypotheses.

CONCLUSIONS

The chemostratigraphic record of the Yujingzi Basin provides data to constrain the age of the fossiliferous Early Cretaceous Xinminpu Group. Three general facies are described that are interpreted to represent deposition of an alluvial fan, which transitioned to lacustrine-to-palustrine paleoenvironments with poorly to moderately drained soils, followed by transition to fluvial-overbank environments with well-drained soils. The majority of the dinosaur fossils occur in the uppermost lacustrine to palustrine facies and in the fluvial-overbank facies. These are interpreted to represent the uppermost Xiagou Formation and the lower Zhonggou Formation within the Xinminpu Group. Previous work suggested that these strata could span the Barremian to Albian. The data presented here constrain the Xinminpu Group in the Yujingzi Basin to the Aptian to early Albian by identifying a broad positive isotope excursion corresponding to carbon isotope segments C9 through C11 of Bralower et al. (1999). The broad C10 positive carbon isotope excursion has previously been associated with OAE 1b and is thought to coincide with global climate changes, and our data provide motivation to identify any continental expression of these changes. Future investigation of paleoclimate proxies from the Yujingzi Basin will elucidate changes in continental paleoclimate.

ACKNOWLEDGMENTS

The authors gratefully acknowledge assistance in the field provided by students and staff of the Fossil Research and Development Center, Third Geology and Mineral Resources Exploration Academy, Gansu Provincial Bureau of Geology and Mineral Development, as well as E. Morschhauser, C. Sartin, and Brandon Hendricks. Funding for travel was provided by the National Science Foundation award no. EAR 1024671 to P. Dodson, H.-L. You, and D. Li. Support was also given by the National Natural Science

Foundation of China (41688103, 41472020, 40672007, 41072019), and the Hundred Talents Project of the Chinese Academy of Sciences to H.-L. You.

ORCID

Hailu You  <http://orcid.org/0000-0003-2203-6461>

LITERATURE CITED

- Baczynski, A. A., F. A. McInerney, S. L. Wing, M. J. Kraus, J. I. Bloch, D. M. Boyer, R. Secord, P. E. Morse, and H. C. Fricke. 2013. Chemostratigraphic implications of spatial variation in Paleocene-Eocene Thermal Maximum carbon isotope excursions, SE Bighorn Basin, Wyoming. *Geochemistry, Geophysics, Geosystems* 14:4133–4152.
- Birkeland, P. W. 1999. *Soils and Geomorphology*. Oxford University Press, Oxford, U.K., 430 pp.
- Breecker, D. O., Z. D. Sharp, and L. D. McFadden. 2009. Seasonal bias in the formation and stable isotopic composition of pedogenic carbonate in modern soils from central New Mexico, U.S.A. *Geological Society of America Bulletin* 121:630–640.
- Bralower, T. J., E. CoBabe, B. Clement, W. V. Sliter, C. L. Osburn, and J. Longoria. 1999. The record of global change in mid-Cretaceous (Barremian-Albian) sections from the Sierra Madre, Northeastern Mexico. *Journal of Foraminiferal Research* 29: 418–437.
- Chen, J., and H. Yang. 1996. Geological development of the northwest China basins during the Mesozoic and Cenozoic; pp. 39–62 in Z. Zhiyi and W. T. Dean (eds.), *Phanerozoic Geology of Northwest China*. Science Press, Beijing, China.
- Ekart, D. D., T. E. Cerling, I. P. Montañez, and N. J. Tabor. 1999. A 400 million year carbon isotope record of pedogenic carbonate: implications for paleoatmospheric carbon dioxide. *American Journal of Science* 299:805–827.
- Enos, P. 1991. Sedimentary parameters for computer modeling; pp. 63–99 in *Computer Simulations and Methods for Improved Parameter Definition*. Bulletin 233, Kansas Geological Survey, Lawrence, Kansas.
- Friedrich, O., H. Nishi, J. Pross, G. Schmiedl, and C. Hemleben. 2005. Millennial-to centennial-scale interruptions of the Oceanic Anoxic Event 1b (Early Albian, mid-Cretaceous) inferred from benthic foraminiferal repopulation events. *Palaios* 20:64–77.
- Föllmi, K. B. 2012. Early Cretaceous life, climate and anoxia. *Cretaceous Research* 35:230–257.
- Gröcke, D. R., S. P. Hesselbo, and H. C. Jenkyns. 1999. Carbon-isotope composition of Lower Cretaceous fossil wood: ocean-atmosphere chemistry and relation to sea-level change. *Geology* 27: 155–158.
- Google Earth. 2015. 40.633683, 98.287372, imagery date September 25, 2011. Available at earth.google.com. Accessed May 18, 2015.
- Hasegawa, H. R., Tada, X. Jian, Y. Suganuma, S. Imsamut, P. Charusiri, N. Ichinnorov, and Y. Khand. 2012. Drastic shrinking of the Hadley circulation during the mid-Cretaceous Supergreenhouse. *Climate of the Past* 8:1323–1337.
- Hay, W. W., and S. Floegel. 2012. New thoughts about the Cretaceous climate and oceans. *Earth-Science Reviews* 115:262–272.
- Heimhofer, U., P. A. Hochuli, S. Burla, N. Andersen, and H. Weissert. 2003. Terrestrial carbon-isotope records from coastal deposits (Algarve, Portugal): a tool for chemostratigraphic correlation on an intrabasinal and global scale. *Terra Nova* 15:8–13.
- Hou, L., and Z.-C. Liu. 1984. A new fossil bird from Lower Cretaceous of Gansu and early evolution of birds. *Scientia Sinica* 27: 1296–1302.
- Jahren, A. H., N. C. Arens, G. Sarmiento, J. Guerrero, and R. Amundson. 2001. Terrestrial record of methane hydrated dissociation in the Early Cretaceous. *Geology* 29:159–162.
- Jenkyns, H. C. 2003. Evidence for rapid climate change in the Mesozoic-Paleogene greenhouse world. *Philosophical Transactions of the Royal Society A: Mathematical, Physical and Engineering Sciences* 361:1885–1916.

- Jenkyns, H. C. 2010. Geochemistry of ocean anoxic events. *Geochemistry, Geophysics, Geosystems* 11:Q03004.
- Ji, S.-A., J. Atterholt, J. K. O'Connor, M. C. Lamanna, J. D. Harris, D.-Q. Li, H.-L. You, and P. Dodson. 2011. A new, three-dimensionally preserved enantiornithine bird (Aves: Ornithothoraces) from Gansu Province. *Zoological Journal of the Linnean Society* 162:201–219.
- Jerzykiewicz, T., and D. A. Russell. 1991. Late Mesozoic stratigraphy and vertebrates of the Gobi Basin. *Cretaceous Research* 12: 345–377.
- Koch, P. 1998. Isotopic reconstruction of past continental environments. *Annual Review of Earth and Planetary Sciences* 26: 573–613.
- Li, D.-Q. 2008. Therizinosauroid dinosaurs from the Early Cretaceous of Yujingzi Basin, Jiuquan area, Gansu Province, China. Ph.D. dissertation, China University of Geosciences, Beijing, China, 118 pp.
- Li, X., W. Xu, W. Liu, Y. Zhou, Y. Wang, Y. Sun, and L. Liu. 2013. Climatic and environmental indications of carbon and oxygen isotopes from the Lower Cretaceous calcrite and lacustrine carbonates in Southeast and Northwest China. *Palaeogeography, Palaeoclimatology, Palaeoecology* 385:171–189.
- Lloyd, G. T., K. E. Davis, D. Pisani, J. E. Tarver, M. Ruta, M. Sakamoto, D. W. E. Hone, R. Jennings, and M. J. Benton. 2008. Dinosaurs and the Cretaceous Terrestrial Revolution. *Proceedings of the Royal Society B, Biological Sciences* 275: 2483–2499.
- Ludvigson, G. A., R. M. Joekel, L. A. González, E. L. Gulbranson, E. T. Rasbury, G. J. Hunt, J. I. Kirkland, and S. Madsen. 2010. Correlation of Aptian-Albian carbon isotope excursions in continental strata of the Cretaceous foreland basin, Eastern Utah, U.S.A. *Journal of Sedimentary Research* 80:955–974.
- Ludvigson, G. A., R. M. Joekel, L. R. Murphy, D. F. Stockli, L. A. Gonzalez, C. A. Suarez, J. I. Kirkland, and A. Al-Suwaidi. 2015. The emerging terrestrial record of Aptian-Albian global change. *Cretaceous Research* 56:1–24.
- McInerney, F. A., and S. L. Wing. 2011. The Paleocene-Eocene thermal maximum: a perturbation of carbon cycle climate, and biosphere with implications for the future. *Annual Reviews of Earth and Planetary Sciences* 39:489–516.
- Menegatti, A. P., H. Weissert, R. S. Brown, R. V. Tyson, P. Farrimond, S. Stasser, and M. Caron. 1998. High-resolution $\delta^{13}\text{C}$ stratigraphy through early Aptian “Livello Selli.” *Paleoceanography* 13:530–545.
- Midwood, A. J., and T. W. Boutton. 1998. Soil carbonate decomposition by acid has little effect on $\delta^{13}\text{C}$ of organic matter. *Soil Biology and Biogeochemistry* 30:1301–1307.
- Morschhauser, E. M. 2012. The anatomy and phylogeny of *Auroraceratops* (Ornithischia: Ceratopsia) from the Yujingzi Basin of Gansu Province, China. Ph.D. dissertation, University of Pennsylvania, Philadelphia, Pennsylvania, 647 pp.
- Nan, P., H.-W. Kuang, and Y.-Q. Liu. 2011. Sedimentary evolution and paleogeography of the Early Cretaceous basins from the northern Qilian Mountains to Jiuxi areas. *Earth Science Frontiers* 18:77–87.
- Ogg, J. G., and L. A. Hinnov. 2012. Cretaceous; pp. 793–853 in F. M. Gradstein, J. G. Ogg, M. D. Schmitz, and G. M. Ogg (eds.), *The Geologic Time Scale 2012*. Elsevier, New York.
- Retallack, G. J. 1997. *A Colour Guide to Paleosols*. John Wiley and Sons, New York, 175 pp.
- Retallack, G. J. 2009. Greenhouse crises of the past 300 million years. *Geological Society of America Bulletin* 121:1441–1455.
- Robinson, S. A., and S. P. Hesselbo. 2004. Fossil-wood carbon-isotope stratigraphy of the non-marine Wealden Group (Lower Cretaceous, southern England). *Journal of the Geological Society, London* 161:133–145.
- Ruddiman, W. F. 2008. *Earth's Climate: Past and Future*, second edition. W. H. Freeman and Company, New York, 388 pp.
- Samaritani, E. J., B. F. Shrestha, E. Frossard, F. Gillet, C. Guenat, P. A. Niklaus, K. Tockner, E. A. D. Mitchell, and J. Luster. 2011. Heterogeneity of soil carbon pools and fluxes in a channelized and a restored floodplain section (Thur River, Switzerland). *Hydrology and Earth System Sciences Discussions* 8:1059–1091.
- Schindler, D. E. 1980. Microstratigraphic sampling and the limits of paleontologic resolution. *Paleobiology* 6:408–426.
- Schlanger, S. O., and H. C. Jenkyns. 1976. Cretaceous oceanic anoxic events: causes and consequences. *Geologie en Mijnbouw* 55: 179–184.
- Scholle, P. A., and M. A. Arthur. 1980. Carbon isotope fluctuations in Cretaceous pelagic limestones: potential stratigraphic and petroleum exploration tool. *AAPG Bulletin* 64:67–87.
- Sewall, J. O., R. S. W. van de Wal, K. van Der Zwan, C. van Oosterhout, H. A. Dijkstra, and C. R. Scotese. 2007. Climate model boundary conditions for four Cretaceous time slices. *Climate of the Past* 3:647–657.
- Srivastava, P. 2001. Paleoclimatic implications of pedogenic carbonates in Holocene soils of the Gangetic Plains, India. *Palaeogeography, Palaeoclimatology, Palaeoecology* 172:207–222.
- Sun, G., D. L. Dilcher, H. Wang, and Z. Chen. 2011. A eudicot from the Early Cretaceous of China. *Nature* 471:625–628.
- Tang, F., Z.-X. Luo, Z.-H. Zhou, H.-L. You, A. Georgi, Z.-L. Tang, and X.-Z. Wang. 2001. Biostratigraphy and palaeoenvironment of the dinosaur-bearing sediments in Lower Cretaceous of Mazongshan area, Gansu Province, China. *Cretaceous Research* 22:115–129.
- Wang, M., D. Li, J. O'Conner, Z. Zhou, and H. You. 2015. Second species of enantiornithine bird from the Lower Cretaceous Changma Basin, northwestern China with implications for the taxonomic diversity of the Changma avifauna. *Cretaceous Research* 55: 56–65.
- You, H.-L., J. O'Conner, L. M. Chiappe, and J. Qiang. 2005. A new fossil bird from the early Cretaceous of Gansu Province, northwestern China. *Historical Biology* 17:7–14.
- You, H.-L., J. Atterholt, J. K. O'Connor, J. D. Harris, M. C. Lamanna, and D.-Q. Li. 2010. A second Cretaceous ornithuromorph bird from the Changma Basin, Gansu Province, northwestern China. *Acta Palaeontologica Polonica* 55:617–625.
- You, H.-L., M. C. Lamanna, J. D. Harris, L. M. Chiappe, J. O'Conner, S. Ji, J. Lu, C. Yuan, D. Li, X. Zhang, K. J. Lacovara, P. Dodson, and Q. Ji. 2006. A nearly modern amphibious bird from the early Cretaceous of northwest China. *Science* 312:1640–1643.
- Vincent, S. J., and M. B. Allen. 1999. Evolution of the Minle and Chaoshui basins, China: implications for the Mesozoic strike-slip basin formation in central Asia. *Geological Society of America, Bulletin* 111:725–742.

Submitted February 7, 2016; revisions received July 31, 2017; accepted March 8, 2018.

Memoirs editor: Randall Irmis.